Available online at www.sciencedirect.com

ScienceDirect

Advances in Space Research 64 (2019) 765–778

ADVANCES IN SPACE RESEARCH (a COSPAR publication)

www.elsevier.com/locate/asr

Transient nature of radio source NVSS J1957+35

Sabyasachi Pal [a,b,*], Dusmanta Patra [b], Monique Hollick [c,d], Sandip K. Chakrabarti [b]

[a] Midnapore City College, Kuturiya, Bhadutala 721129, India
[b] Indian Centre for Space Physics, 43 Chalantika, Garia St. Road, Kolkata 700084, India
[c] Defense Science and Technology Group, West Avenue, Edinburgh, South Australia 5111, Australia
[d] University of New South Wales, Anzac Parade, Kensington, NSW 2052, Australia

Received 3 November 2018; received in revised form 6 May 2019; accepted 9 May 2019
Available online 18 May 2019

Abstract

We have searched for transient and variable radio sources in the field of Galactic micro-quasar Cygnus X-1 near 1.4 GHz (L band) using data from the Karl G. Jansky Very Large Array. We used twenty years of data between 1983 and 2003. We found a source NVSS J1957+35 showing transient behavior. The source was also mentioned earlier in NVSS and WENSS catalog but its transient nature was not reported earlier. The source is located 23.8 arcminutes far from Cygnus X-1. It is detected many times during the span of our study and it varied between less than 1.9 mJy (3σ) to 201 mJy. NVSS J195754+353513 also showed high intra-day variability. In one occasion, the source rose from ~15 mJy to ~170 mJy within 700 s. We detected circularly polarized emission from the source for a limited number of cases with fractional circular polarization varies between 0.14 and 0.17. 2MASS J19575420+3535152 may be the near-infrared counterpart of the source. We compared the properties of the source with other Galactic transient sources having similar properties. The nature of the source is still unknown. We discussed the possible nature of the source.

Keywords: Radio continuum: general; Radio continuum: transients; Radio continuum: stars; Stars: flare; Stars: variables: general

1. Introduction

The dynamic radio sky is not studied in detail due to one or more reasons like lack of telescopes with a large field of view, observational constraints, band width etc while the steady state radio sky is considerably well studied and modeled (e.g., Becker et al., 1995; Condon et al., 1998). There are various types of sources which show variability at different time scales. For example, brown dwarfs, flaring stars, masers, pulsars, micro-quasars, supernovae, gamma-ray bursts and active galactic nuclei show high levels of variability (e.g., Cordes et al., 2004, for a review). Until recently there are only a few radio surveys which searched for variable and transient radio sources efficiently (e.g., see, Gregory and Taylor, 1986; Matsumura et al., 2009). So, most of the radio transients have been found through follow-up observations of known or suspected transient emitters.

The recent programs to search for radio transients from direct and archival observations revealed some potential radio transients which are consistent with the expectation that previous limitations on the detection of radio transients were instrumental and not astrophysical. For example, a giant burst was detected from a young stellar object (Bower et al., 2003). Many 1–3 Jy radio bursts were found at high and low Galactic latitudes (Niinuma et al., 2007; Matsumura et al., 2007; Kida et al., 2008). A periodic, coherent and circularly polarized burst was found in an ultra-cool dwarf (Hallinan et al., 2007). A few tens of Fast Radio Bursts (FRBs) have been detected so far which

* Corresponding author at: Midnapore City College, Kuturiya, Bhadutala 721129, India.
E-mail address: sabya.pal@gmail.com (S. Pal).

https://doi.org/10.1016/j.asr.2019.05.014
0273-1177/

lasted only for a few milliseconds (e.g., Lorimer et al., 2007; Ravi et al., 2016). The origin of FRBs is still unclear but due to relatively high dispersion measures, some believe these sources have an extra-galactic origin (e.g., Lorimer et al., 2007). The recent discovery of repeated bursts from FRB 121102 by Arecibo Telescope (Spitler et al., 2014; Spitler et al., 2016) and corresponding follow-up interferometric observations (Chatterjee et al., 2017; Marcote et al., 2017) showed that the location of at least this FRB coincides with the star-forming region of a low-metallicity dwarf galaxy at red-shift $z = 0.193$ (Bassa et al., 2017; Tendulkar et al., 2017).

Huge improvements in the field of view, especially at low radio frequencies, helps to study transient and variable radio sources more effectively (e.g., Macquart, 2014). However, no detection of any transient sources from recent 12,000 deg^2 systemic transient search comprising of 2800 pointings using the Jansky Very Large Array Low-band Ionosphere and Transient Experiment (VLITE) (Polisensky et al., 2016) and detection of only one transient source from monitoring of region close to the north celestial pole (Stewart et al., 2016) covering 175 deg^2 using the Low-Frequency Array (LOFAR) and no detection of transient source from 1430 deg^2 search using Murchison Widefield Array (MWA) (Bell et al., 2014; also see the MWA study by Rowlinson et al. (2016)) show that detections of transient radio sources are currently not very common, especially at low radio frequencies. Future deep, wide-field searches may potentially be far more fruitful (e.g., recent transient rate calculations in Metzger et al., 2015; Mooley et al., 2016).

Large archival data from various telescopes are an important resource to look for transient and variable radio sources. Earlier, Bannister et al. (2011) reported 15 transient sources from the study of 22 year archival data of the Molonglo Observatory Synthesis Telescope covering 2776 deg^2 survey area. Recently, Murphy et al. (2017) found a candidate transient source at low frequency from a comparison of TIFR GMRT Sky Survey Alternative Data Release 1 (TGSS ADR1, see Intema et al., 2017) and the GaLactic and Extragalactic All-sky Murchison Widefield Array (GLEAM, see Hurley-Walker et al., 2017) survey catalogues. Ten milli Jansky level transients were detected from the archival data of 22 years the Karl G. Jansky Very Large Array (VLA) observations of a single field-of-view at 5 and 8.4 GHz (Bower et al., 2007). Later Frail et al. (2012) showed that more than half of the transient sources reported in Bower et al. (2007) were due to data artifacts and rest of the sources had a low signal-to-noise ratio (S/N) than Bower et al. (2007) to conclusively determine transient nature of these sources. Many variable and transient radio sources were reported from archival data search of the NRAO VLA Sky Survey (NVSS) (Condon et al., 1998) and Faint Images of the Radio Sky at Twenty-cm (FIRST) (Becker et al., 1995) survey (Levinson et al., 2002; Thyagarajan et al., 2011).

Earlier detection of two Galactic Centre Radio Transient (GCRT) sources GCRT J1745-3009 (Hyman et al., 2005; Hyman et al., 2007; Roy et al., 2010) and GCRT J1742-3001 (Hyman et al., 2009) were made from a systematic search of near Galactic Center region using the VLA and the Giant Meterwave Radio Telescope (GMRT). GCRT J1745-3009 is a unique source which was detected only three times in 2002 (Hyman et al., 2005), 2003 and 2004 (Hyman et al., 2007). The properties of the source changed significantly between three detections of the source. In 2002, this source exhibited ~10 min long, ~1 Jy peaked bursts with a ~77 min period. The emission from the source was coherent (Hyman et al., 2005). Extremely steep spectral index ($\alpha = -13.5 \pm 3.0$) (Hyman et al., 2007), and high circular polarization (Roy et al., 2010) was found from the third detection of the source. All the three detections of the source were in 330 MHz. The characteristics of GCRT GCRT J1745-3009 did not match with any known mechanisms of emission in transient compact sources. As a result, the source seems to represent a member of a new class of coherently emitting objects. GCRT J1742-3001 was active for a few months with ~150 mJy flux density at the peak and showed no periodicity in emission (Hyman et al., 2009). The source was detected in 235 MHz and exhibited a steep spectral index ($\alpha < -2$). For both of these sources, no counterpart was discovered in the high energy, ruling out the possibility of conventional follow-up radio observations after a high-energy detection. Another Galactic Center radio Transient (GCT) was detected close to the Galactic center region with high variability which was in an active phase for a few months (Zhao et al., 1992).

In this paper, we look for new variable/transient sources from a single well observed field centered at micro-quasar Cygnus X-1. Though we could not detect a new source, we discovered hitherto un-reported transient behavior of one NVSS source, namely, NVSS J195754+353513 (J1957+35 hereafter). This source is located approximately 23.8 arcminutes far from the micro-quasar Cygnus X-1 at J2000 co-ordinates $\alpha = 19\text{h}57\text{m}54.12\text{s}$ ($\pm 0.04s$), $\delta = +35^\circ 35' 13.7''$ ($\pm 0.6''$). In Section 2, we summarize observational details and data analysis procedure. In Section 3, we summarize various results of the source. We discuss the significance of various findings in Section 4. Finally, we make concluding remarks in Section 5. In this paper, we used the convention of spectral index α as $S_\nu \propto \nu^\alpha$.

2. Observation and data analysis with the Karl G. Jansky very large array

A blind search for new variable radio sources was conducted using archival VLA data[1] at the L-band. L band is suitable for this kind of search with the VLA as it provides an acceptable balance between field of view and sen-

[1] https://science.nrao.edu/facilities/vla/archive/index.

sitivity. Though the field of view in 74 and 325 MHz bands with the VLA will be larger, these bands have poorer sensitivity. There is also less amount of available archival data in the frequencies smaller than L band. The central frequency of observations presented in this paper is either 1.3851 GHz or 1.4649 GHz.

VLA comprises twenty-seven fully steerable antennas each with 25-meter diameter in a Y-shaped array. Antennas are periodically moved in a different configuration to achieve different scientific goals where the most expanded antenna configuration is known as A configuration and the most compact one is D configuration. B and C configurations are intermediate between A and D. Occasionally antennas are placed in a hybrid configuration, like AB or BC when some of the antennas are in one configuration and some of them in other. The maximum size of the baselines B_{max} in A, B, C and D configurations are 36.4, 11.1, 3.4 and 1.03 km respectively which corresponds to synthesized beam-width θ_{HPBW} 1.4, 4.6, 15 and 49 arc-sec respectively at 1400 MHz.

The data used for the present work was taken from different configurations of the VLA between 12 October 1983 (MJD 45619) and 4 June 2003 (MJD 52794). In total, we have used 262 different epochs of observations with various intervals ranging from days to years between successive observations. The antennas were in configuration A, AB, AD, B, BC, C, CD, and D for 53, 16, 5, 46, 15, 45, 26, and 56 days, respectively.

We studied a field centered on Cygnus X-1, a radio emitting X-ray binary (Bowyer et al., 1965; Giacconi et al., 1972; Webster and Murdin, 1972; Bolton, 1972) with coordinates 19h58m21.676s+35°12′05.78″ (J2000). This area of the sky was chosen because the field of Cygnus X-1 is one of the best studied Galactic black hole binaries using VLA due to the fact that it is the first system widely accepted to contain a black hole (Murdin and Webster, 1971; Tananbaum et al., 1972; Gies and Bolton, 1986). This makes the field ideal for looking variable/transient sources.

There are big data gaps between April 1986 to April 1988, May 1991 to October 1996 as well as February 2001 to June 2003. The 'on source' observation time in each epoch was between 2 and 15 min for most of the days with median and mean observation time of 2.5 and 11.4 min. Observing bandwidth for most of the days was 50 MHz using a single channel.

Analysis and imaging of the data were carried out with the Astronomical Image Processing System (AIPS).[2] Bad data were flagged. Perley and Butler (2013) flux density scale was used. For eighteen epoch of observations, the quality of data was not good and we could not make reasonably good images. We did not use the data for these days. While using data for CD and D configuration, we used lower *uv* cut-off to avoid strong background extended radiation from the Galactic plane. We have made the correction for the primary beam using AIPS task PBCOR.

Amplitude calibration was conducted in reference to 3C 286 and phase calibration was based on observations of the nearby source J2007+404 or J2015+371. We have not performed self calibration due to lack of any strong point source in the field. The integration time used for solving amplitude and phase during calibration was 10 s. The images of different days have variable noise levels. The noise level near the source location increased due to primary beam correction as the source is 23.8′ far from the field center where the half power beam width of the VLA primary beam at 1.4 GHz is 32″. Also, small on-source time for most of the individual observation resulted in a high noise level. The median value of noise level near the source position was 1.8 mJy beam^{-1}. The noise level in individual days varied between 0.26 mJy beam^{-1} and 18.7 mJy beam^{-1}.

To model the steady state sky around the field of interest, two models were created combining all data of similar Intermediate Frequencies (IFs). The first model (model 1) was created with 94 epoch of observations with IF 1.3851 GHz and the second model (model 2) was created with 18 epoch of observations with IF 1.4649 GHz. To look for variable sources, steady-state model with similar frequency configuration was subtracted with individual single epoch observations using the AIPS task UVSUB. Only variable sources should be visible in individual steady state sky substracted images. Apart from Cygnus X-1, we found that only one source NVSS J1957+35 is present in many of the subtracted images with significantly fluctuating flux. The subtracted flux density for NVSS J1957+35 was up to ∼120 mJy. The noise levels close to the location of NVSS J1957+35 in model 1 and model 2 were 0.19 mJy beam^{-1} and 0.46 mJy beam^{-1} respectively.

3. Result

3.1. Detection of NVSS J1957+35

We have detected a transient radio source which is showing high variability with the different temporal scale of variation. The source is showing variation between 1.9 mJy (3σ) to 175.3 mJy in most compact D configuration of VLA, where the effect of smearing was minimal. The location of the source is 19h57m54.3s (± 0.8s) +35°34′59.6″ (± 0.6″) (J2000). The location is measured by averaging all the position estimations from individual observation where the estimation from individual observation is done by fitting an elliptical Gaussian around the peak of the source, along with a background level to the source. The error in the position mentioned above is the standard deviation of 1σ uncertainty in the fitting. After cross-correlation of the measured position of the transient source with NVSS sources, we found the transient source detected by us is NVSS J195754+353513. Since the posi-

[2] http://www.aips.nrao.edu.

tion measurements of the source presented above may have large error due to band-width smearing (effect of which is discussed later part of this section in detail), we have used NVSS position $\alpha = 19h57m54.12s$, $\delta = +35°35'13.7''$ (J2000) of the source (Condon et al., 1998) for further study. The corresponding Galactic co-ordinates are $l = 71.6°, b = 3.3°$.

In Fig. 1, examples of images of NVSS J1957+35 are shown during observations in different VLA configurations and time. The images of the source in B configuration on 7th November 1999 and 11th February 2000 are shown in the upper left and upper right panels of the Figure. In the middle left, middle right and lower left panels, we have shown examples of detection of the source in A, C and D configurations of VLA. In the lower right panel, an example of no detection is shown when VLA was in C configuration. The observation details and different image parameters corresponding to Fig. 1 are summarized in Table 1.

The location of NVSS J1957+35, as per the NVSS catalog, is shown in all images of Fig. 1. The NVSS J1957 +35 coordinates are consistent with the location of the generally extended emission in the present study of archival VLA observations. NVSS survey is carried out using D configuration of VLA and the source is unresolved in NVSS with flux density of 50.8 ± 1.6 mJy at L band (Condon et al., 1998). It was not resolved during our study also when it was observed in D configuration. For example, the major and minor axises of Gaussian fitting on 18th March 1991 (which is shown in lower-left hand panel of Fig. 1) are 27.8″ and 18.4″ which is less than synthesized beam ($37.5'' \times 32.6''$) of the observation.

A transient source should be point like. The elongation of the source visible in Fig. 1 with average positional angle 166 degree east from the north is most probably not due to intrinsic source structure but an effect of bandwidth smearing due to a high channel width of 50 MHz. The direction of elongation of the source, as visible in Fig. 1, is towards the pointing center which is a signature of bandwidth smearing. In all the images, the source is consistently elongated in the same direction, when detected.

The reduction in the peak flux density due to bandwidth smearing effect could be calculated using the following formula (Bridle and Schwab, 1999)

$$1 - R_{\Delta\nu} = 1 - \frac{I}{I_0} = 1 - \frac{\sqrt{\pi}}{\gamma\beta} erf \frac{\gamma\beta}{2} \quad (1)$$

where I_0 is the peak response for $\Delta\nu = 0, I$ is the peak of the degraded response of the source and $\beta = \frac{\Delta\nu}{\nu_0}\frac{\theta_0}{\theta_{HPBW}}$. Here ν_0 is observing frequency, $\Delta\nu$ is the bandwidth of the emission used for imaging, θ_0 is the angular distance of a source from the field center and θ_{HPBW} is the half power beam width. Here erf is the usual error function and $\gamma = 2\sqrt{ln2}$. The calculated reduction in peak flux densities for the VLA A, B, C and D configurations with 50 MHz bandwidth are 97%, 91%, 71% and 33% respectively. The reduction due to time-average smearing (Bridle and Schwab, 1999) in A, B, C and D configurations are 17%, 1.6%, 0.14% and 0.01% respectively. Though the effect of smearing is large in VLA configuration with longer baselines, it does not affect the integrated flux density provided all the smeared out flux is recovered. We have studied the temporal variation of the source using integrated flux-density which has no effect on smearing. However, we may miss some of the detections in longer baselines when the smeared out peak flux density is less than the detection threshold. Probably this is the reason for the lower detection rate of the source in A configuration comparable to others. For the high resolution observation using configuration A, B and AB where the smearing effect is significant, it is possible that source is so smeared out that all of the flux can not truly be recovered and the corresponding measurement should be treated as a lower limit. The fact that the source showed significant flux-density variation within measurements from the same configurations indicates that the variation is real.

It is also possible that (though with very less probability) the elongation towards the pointing center of the image, as visible in Fig. 1, is partly due to the intrinsic structure of the source. The causality argument defines a relation between the variability time and the size of the emission region which produces the variation. Based on the observed short time-scale, in the majority of the cases, even if the source is extended, the origin of the variable emission is still in a compact region. This is common for many of the extended sources like microquasars (Mirabel and Rodriguez, 1998). Further pointed observation on the source location is required to confirm the structure of the source.

To be sure that the variation of NVSS J1957+35 is not due to any kind of systematic effects or error in amplitude calibration, we measured flux density of another source NVSS J195823+345728 present in our field. The recorded flux density of the source in the NVSS catalog is 52.3 ± 1.6 mJy (Condon et al., 1998). We found that during our study, the mean and median integrated flux density of the source were 50.8 and 51.7 mJy respectively. The standard deviation in measurements of flux-densities of the source was 5.2 mJy which means the percentage of deviation was 10.2%. This shows error in amplitude calibration plays little role in the large variation of NVSS J1957+35. NVSS J195823+345728 is located 14.6 arc-min far from the phase center. The reduction in the peak flux density due to bandwidth smearing effect (R) for NVSS J195823+345728, corresponding to VLA A, B, C and D configurations are 96%, 87%, 62% and 19% respectively. The difference between median flux-densities corresponding to the VLA configuration A (which was heavily smeared due to band-width and time-smearing) and that of the VLA configuration D is less than 5% of total flux-density of the source. This shows that the smearing has little effect on the measurement of integrated flux-densities.

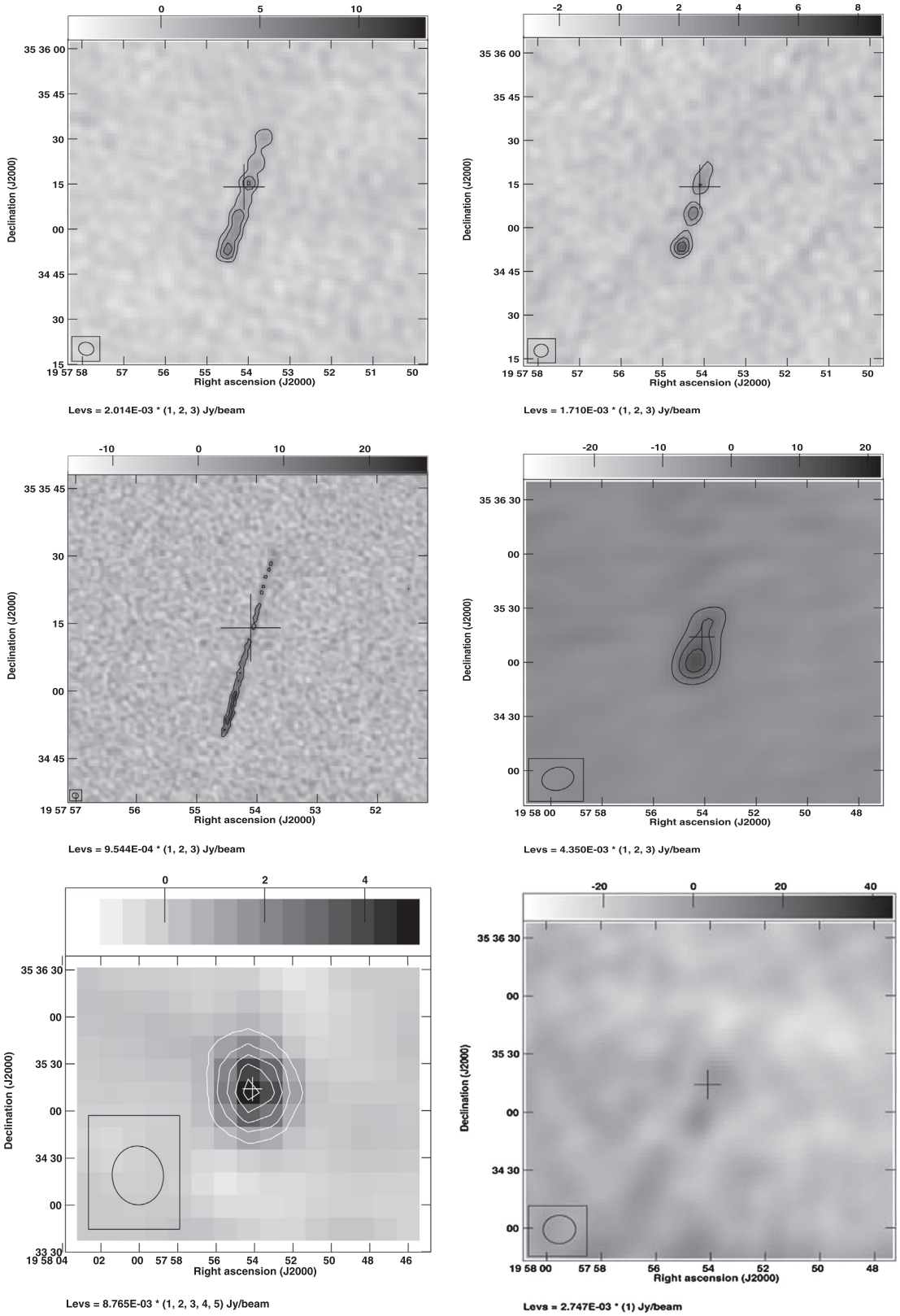

Fig. 1. Images of NVSS J1957+34 in different configurations of VLA at L band. In the upper left and right panels, we have shown images of the source in B configuration on two different dates. In the middle left, middle right and lower left panels, we have shown examples of detection of the source in A, C and D configurations of VLA. In the lower right panel, we have shown an example of no detection when VLA was in C configuration. We have included the synthesized beam at the left-bottom corner of each panel. The location of the NVSS position is shown by a cross in all the images where the size of the cross is an error in NVSS location multiplied by 10 for easy visualization. The unit of the grey-scale bars at the top of each panel are mJy beam^{-1}. For details, see text and Table 1.

Table 1
Details of observations corresponding to Fig. 1.

Image location	Date (MJD)	Configuration	Flux density (mJy)	RMS (mJy-beam^{-1})	Synthesized beam ($'' \times ''$)	On source time (s)
Upper Left	51489	B	45.9 ± 5.0	0.6	4.60×4.22	170
Upper Right	51585	B	26.8 ± 3.1	0.5	4.44×4.14	120
Middle Left	47954	A	50.3 ± 5.3	0.3	1.28×1.17	13820
Middle Right	45826	C	53.0 ± 5.6	1.7	15.56×12.48	390
Lower Left	48337	D	84.0 ± 8.6	2.0	37.50×32.57	553
Lower Right	50691	C	<16.5	5.5	14.70×14.48	100

Note: 3σ upper limit is mentioned when the source is not detected.

3.2. Radio light curve of NVSS J1957+35

Light curves displaying a variation of the source's flux densities between 1983 and 2003 is shown in Fig. 2. For the VLA configuration C and D, the flux densities are calculated using AIPS task JMFIT using the results of fitting a Gaussian, along with a background level. For the VLA configuration A, B and AB, often the source is showing hints of multiple components and we used AIPS verb TVSTAT to calculate the flux-density of the source. TVSTAT prints mean, rms brightness and flux density of an image within user defined polygon. For the VLA configuration C and other compact configurations, where multiple components of the source are not visible, the difference in measurement by JMFIT and TVSTAT is negligible. The non-detections are reflected by the triangular points in Fig. 2, which correspond to the 3σ upper limits. For the measurements done with configuration A, B and AB using TVSTAT when the source is most of the time resolved, the error bar is calculated as the RMS noise levels of the images near the location of NVSS J1957+35, source extent in number of synthesized beams times the RMS noise level and a 10% uncertainty in the absolute calibration of each data set added in quadrature. For measurements with configuration C, D and CD, the source is not resolved and the error bars represent the RMS noise levels of the images near the location of NVSS J1957+35 and a 10% uncertainty in the absolute calibration of each data set added in quadrature. There are only nineteen observations of the field between MJD 46612 (July, 1986) and MJD 50326 (August, 1996). The source was detected on 161 occasions and not detected on 83 occasions. The data was not good enough to make reasonably good images for 18 days. So, the source was successfully detected for 66.0% days amongst all observations with good data of the field. The source showed multiple short bursts and high variation. It varied from less than 1.9 mJy (3σ) to 201 mJy. The median value of flux density was 38.9 mJy. We have found the average flux density and the corresponding standard deviation 65.2 mJy and 25.6 mJy for the light curve in the left panel of Fig. 2 and 62.9 mJy and 36.5 mJy in the right panel of Fig. 2 respectively. On 25th January 2002 (MJD 52299) NVSS J1957+35 reached maximum value within the observational period reported in this paper with 201 mJy flux density. The source showed the signature of various flares and the peaks reached more than 150 mJy on 23rd July 1998 (186 mJy), 24th March 1999 (175 mJy) and 16th June 2000 (160 mJy).

Due to gaps in the observations, we can study the rising and fading stages of flares only in a few cases. In Fig. 3 we have shown two such flares in March and April-May of 1991 when the peak reached ~85 mJy and ~75 mJy respec-

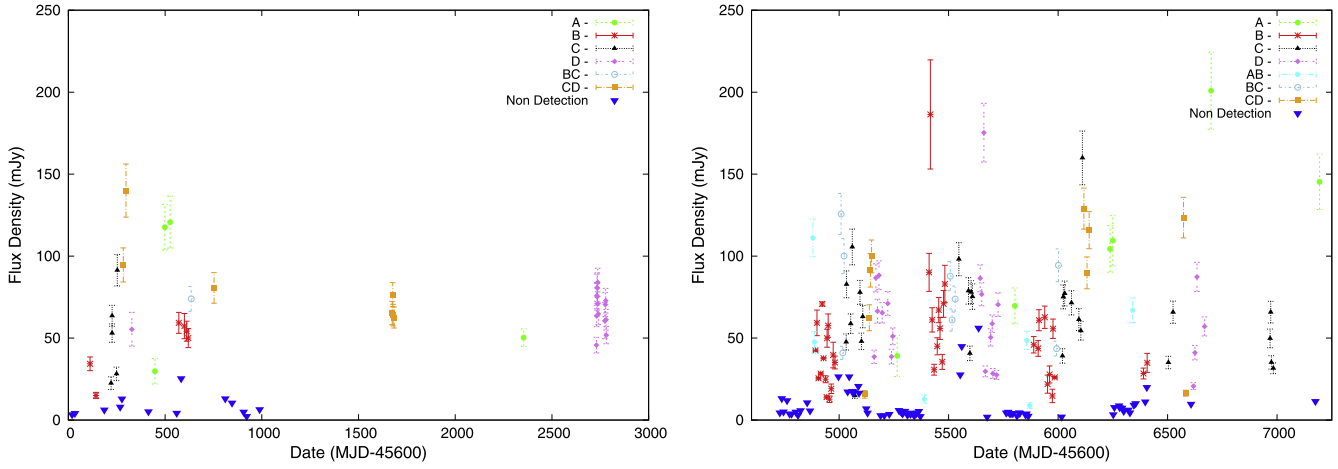

Fig. 2. Light curves of NVSS J1957+35 at L band. In the left panel, the observations between 1983 and 1991 are plotted and in the right panel, the observations between 1996 and 2003 are plotted. The observations are done by the VLA. Here the triangles show days of non-detection with 3σ upper limits.

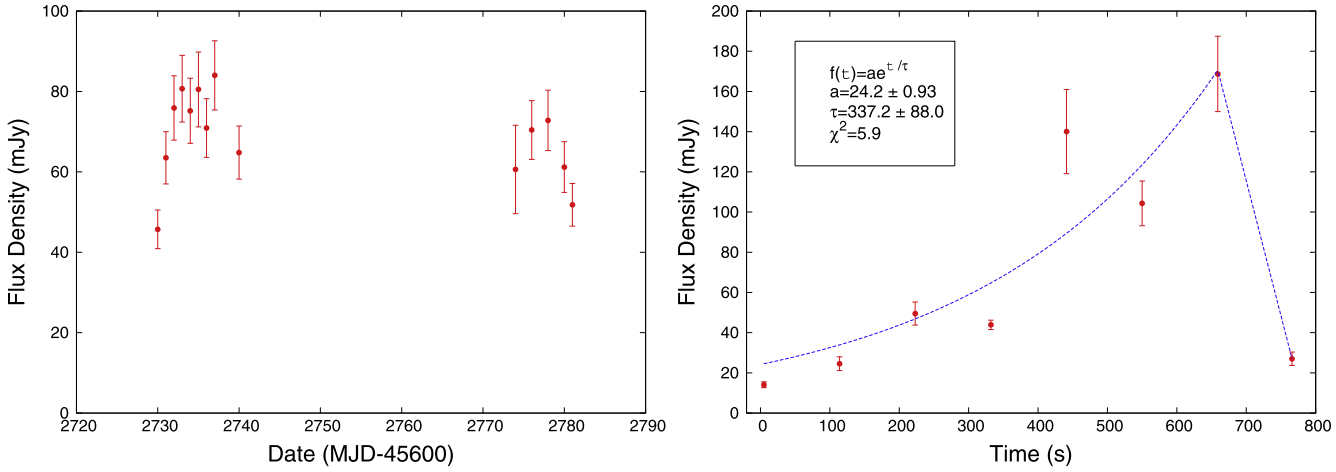

Fig. 3. Left (Inter-day variation): Example of two flares of NVSS J1957+35 observed at L band. These flares were observed in March and April-May 1991. Antennas were in D configuration during these time. Right (Intra-day variation): An example of an intra-day variation of NVSS J1957+35 within a scan. The observation took place on 3rd February 2000 (MJD 51577). Antennas were in B configuration during this observation. Exponential fitting over the points in the rising phase is also shown in the figure. The reduced χ^2 value of the fit is also included.

tively. It is also possible that two bumps in the light-curve are part of the same flaring activity, and the gap in the sampling makes it look like two different flares. Antennas were in D configuration during these times. There were not enough data points to precisely determine life-span and rise/decay rate of these flares. The first flare was detectable between 15th March 1991 to 25th March 1991 and the second flare was detectable between 28th April 1991 to 5th May 1991.

In Fig. 5 we have shown the field of NVSS J1957+35 combining 9 days of observations. All observations used in this Figure were made in 1991 when antennas were in D configuration. The RMS noise of the image was 0.17 mJy beam^{-1} and the resolution of the image was $43.23'' \times 41.71''$. We can see NVSS J1957+35 with 60 mJy flux density along with Cygnus X-1 and many other background sources.

We looked for possible periodicity in NVSS J1957+35 as was found in some other radio transients. The light-curve data was systematically folded with a different period to search for the signature of any periodicity in the emission. No periodicity was found in the source light curve.

There are no available VLA archival data of the source in any other band except L band. Thus a study of the spectral index of the source was not possible using VLA data. There is a source in 325 MHz WENSS (Westerbork Northern Sky Survey; Rengelink et al. (1997)) catalog which is 5.11 arc-sec far from the NVSS position of the source with flux density 67 mJy. Since the positional uncertainty in WENSS for faint sources are ~5 arc-sec, this is most probably the same source. The source has a flat spectral index of $\alpha = -0.19$ between NVSS and WENSS measurements (Massaro et al., 1984). Since the source is highly variable and there is a gap between measurements between NVSS and WENSS (observations of WENSS took place between 1991 and 1996 and observations of NVSS took place between 1993 and 1996), the flat spectral index measured between NVSS and WENSS is misleading.

3.3. Intra-day flux density variation

Based on previous studies of the bursting transient GCRT J1745-3009 (see Section 1 for reference) and GCRT J1742-3001 (Hyman et al., 2009), we searched for flux density variations of NVSS J1957+35 between different scans of the observations of the same day. Since the median on-source observation time for NVSS J1957+35 observation is only 2.5 min and the flux density of the source was not adequate to image it all the time with the small time scale, we could make a study of the intra-day variation only for a limited number of cases.

Significant scan to scan and intra-scan flux density variation is detected when it was possible to image separate scans. In the right hand panel of Fig. 3, we have plotted an example of an intra-day variation of NVSS J1957+35 within a scan. The observation took place on 3rd February 2000 (MJD 51577). Antennas were in B configuration during this observation. The source rose from 15 to 170 mJy within 700 s and then came back to ~27 mJy level within ~100 s. The rise time constant, resulting from the exponential fit over the points in a rising phase, is $\tau = 337 \pm 88$ seconds. A power-law fit ($S_\nu \propto t^\beta$) over points in rising phase of the flare yields $\beta = 1.4 \pm 0.7$. To confirm that the variation is intrinsic to the source and not due to any kind of systematics, we measured the flux density of the nearby background source NVSS J195823+345728. The standard deviation in measurements of flux-densities of NVSS J195823+345728 was 3.1 mJy from its mean measured value of 50.3 mJy, which means the percentage of deviation in the flux-density measurement of this background source was only 6.1% while NVSS J1957+35 changed from 15 to 170 mJy during the same time.

Table 2
Intra-day flux density variation of NVSS J1957+35.

Date (UT) (UT)	1st Scan Time Span (min)	1st Scan Flux Density (mJy)	2nd Scan Span (min)	2nd Scan Flux Density (mJy)	Time gap between scans (min)
03/07/84	6.5	50.9 ± 8.4	6.5	216 ± 22.7	52.5
04/03/90	29.16	204.0 ± 21.6	29	40.2 ± 4.7	204.5
16/03/91	19.0	68.1 ± 7.4	13.5	55.4 ± 6.3	5.5
25/03/91	15.5	88.1 ± 9.7	14.5	37.9 ± 4.6	5.5
16/03/97	0.92	80.8 ± 9.2	0.92	115 ± 11.8	0[a]
25/01/99	1.33	111.0 ± 11.9	1.33	48.4 ± 5.9	0[a]
24/10/02	2.83	37.6 ± 4.6	3.17	76.7 ± 8.7	57.5

[a] Note: Zero difference between two time-spans mean we are looking for intra-scan variations.

In Table 2, we have summarized intra-day flux density variations for different days. Since the variation corresponding to 3rd February 2000 is already shown in details in the right hand panel of Fig. 3, we have not included it in Table 2. The error in flux density mentioned in the table is the RMS noise levels of the images near the location of NVSS J1957+35 and a 10% uncertainty in the absolute calibration of each data set added in quadrature. For six different days, we found more than 20% difference in flux densities between two successive scans of observations with time difference 5.5–204.5 min. On 4th March 1990 (MJD 47954), the flux decayed from 204.0 mJy to 40.2 mJy with just 204.5 min separation and on 3rd July 1984 (MJD 45884), the flux density rose from 50.9 mJy to 216 mJy when the gap between two successive scans were just 5.5 min. For two days, we found significant variation ($> 20\%$) within a scan. Except 3rd February 2000, more than 20% intra-scan flux-density variation with less than 1 min time-scale is not detected. For all the cases, we measured the flux-density of the background source NVSS J195823+345728 and found that the variation in flux-density measurements were always < 7 mJy confirming that the variation in NVSS J1957+35 is intrinsic property of the source and not due to any kind of systematics or error in amplitude calibration.

3.4. Circularly polarized emission

We looked for the presence of circularly polarized emission from NVSS J1957+35 as was found for the case of GCRT J1745-3009 (Roy et al., 2010). The measurement of Stokes V polarization on 19th March 1991 (MJD 48334) was 12.6 mJy with RMS noise of 1.19 mJy beam^{-1} and the measurement of Stokes V polarization on 2nd May 1991 (MJD 48378) was 11.5 mJy with RMS noise of 1.36 mJy beam^{-1}. The corresponding value of V/I on 19th March and 2nd May 1991 were 0.17 ± 0.19 and 0.16 ± 0.22. Relatively weak Stokes V detection was done on 1st December 1999 (MJD 51513) with flux density 8.3 mJy and RMS noise 0.6 mJy beam^{-1}. The corresponding V/I was 0.14 ± 0.17. More than 5σ Stokes V was not detected from data of any other days. Linear polarization properties could not be studied due to the lack of suitable polarization calibrators.

3.5. Optical/IR and X-ray counterpart of the source

There are no known X-ray sources coincident with NVSS J1957+35. Future improvements in X-ray instrumentation or future flaring behavior of the source may help in detecting the X-ray counterpart of the source.

We have searched for the optical/infra-red counterpart of NVSS J1957+35. There are two sources within 10 arc-sec from the source location of NVSS J1957+35 in the Two Micron All-Sky Survey (2MASS) point source catalog (Cutri et al., 2003; Skrutskie et al., 2006). The nearest source in the 2MASS catalog is J19575420+3535152 which is 1.82 arc-sec away from the location of NVSS J1957+35. This may be the near infra-red counterpart of NVSS J1957+35. The other source in 2MASS catalog within 10 arc-sec from NVSS J1957+35 is J19575378+3535221 whose position is 9.37 arc-sec away from NVSS J1957+35. The brightnesses of J19575420+3535152 in J, H and K bands are 15.45, 14.90 and 14.55 mags respectively.

In Fig. 4, we have shown the field of NVSS J1957+35 as observed by the Palomar Observatory Sky Survey II (POSS II) (Cabanela et al., 2003) in the red band. The radio image of 7th November 1999 is overlayed with the optical image and is shown by contours. VLA was in B configuration during this observation. The position of the NVSS source, the location of 2MASS J19575420+3535152 and 2MASS J19575378+3535221 are shown in the image.

It is also possible that the optical/NIR source (as visible in Fig. 4) is a different source than the radio source and just by chance located in the same direction. Since the source is located in a crowded region and just 3.3° far from the Galactic plane, a chance optical/NIR and radio alignment can not be overruled.

4. Discussion

4.1. The nature of the source NVSS J1957+35

We have searched the environment of NVSS J1957+35 for associated discrete sources or extended structures.

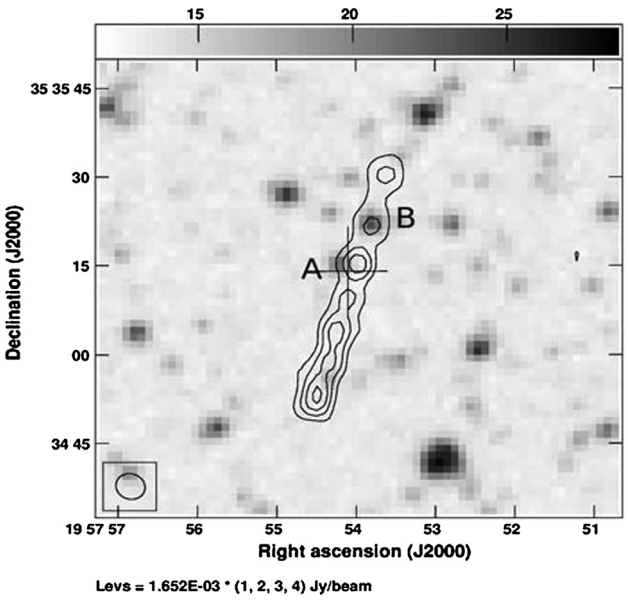

Fig. 4. Optical image of the field of J1957+35 as observed by the Palomar Observatory Sky Survey II (POSS II) in the red band. The image is overlayed with contours in radio. The location of the NVSS position is shown by a cross in the image where the size of the cross is an error in NVSS location multiplied by 10 for easy visualization. Here A represents the location of 2MASS J19575420+3535152 and B represents the location of 2MASS J19575378+3535221.

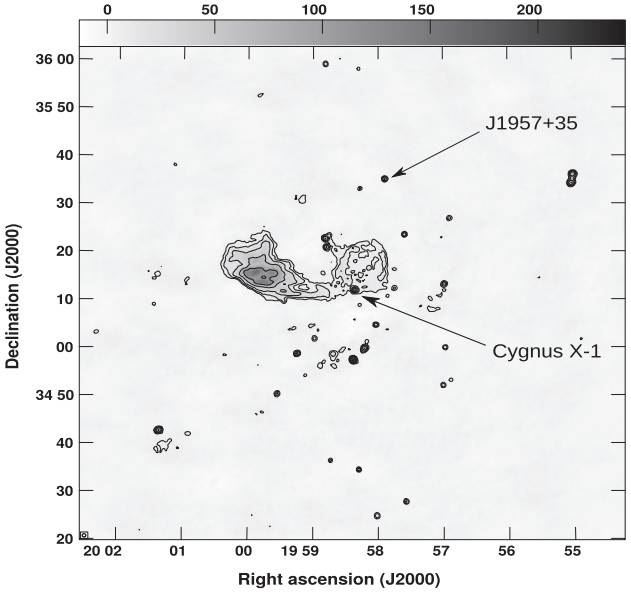

Fig. 5. L band VLA image of the field of NVSS J1957+35 combining 9 days of observations. All observations used in this image were conducted in 1991 when antennas were in D configuration. The RMS noise of the image is 0.17 mJy beam^{-1}. Cygnus X-1 and NVSS J1957+35 are indicated by the arrow. The synthesized beam of the image is 43.24″ × 41.71″. The unit of the grey-scale bar is mJy beam^{-1}.

The source is not close to any known supernova remnant. Except for the elongated structure of the source in longer VLA configurations which is possibly due to various smearing effects (as discussed in detail in Section 3.2), we did not find a trace of any extended structure close to the source.

It is possible that the radio emission of NVSS J1957+35 arises from activities of a foreground flaring star. Many flaring stars are known to exhibit activity in both radio and X-ray wavelengths such as the giant outburst from a young stellar object reported by Bower et al. (2003), but the detection of radio flares having no apparent associated X-ray emission is not uncommon. For example, radio flares from UV Ceti star with seconds to minutes time-scale was detected at low frequencies by Spangler et al. (1974) and Karpen et al. (1977) with YZ Canis Minoris where no corresponding X-ray emission was found. At higher frequencies (4.9 and 8.4 GHz), Osten et al. (2005) reported short duration radio flares from the dMe flare star EV Lacertae which were not clearly related to the star's X-ray flares. The radio flares reported in these stars range from a few milli Jansky to a few tens of milli Jansky, with the rise and decay times of ∼1 min and ∼1 h respectively. We have also found short flares from NVSS J1957+35 of ∼700 s duration as shown in the right-hand panel of Fig. 3.

Richards et al. (2003) presented results on five years of continuous monitoring of radio flares of Algol-type and RS CVn systems; many of the flares reached hundreds of milli Jansky with a few days to a month duration. Numerous short bursts within each flare were also visible. Strong periodic activities are also found in these systems where the shortest periodicity was found in β Per with 48.9 ± 1.7 days. Though we could not detect any periodicity in emission from NVSS J1957+35, the source could be RS CVn system due to the similarity in the time scale of flaring episodes.

Pulsars can produce highly circularly polarized emission in a single pulse (e.g., Kazbegi et al., 1991). There are some pulsars which show non-periodic flaring events like Crab pulsar (e.g., Buehler et al., 2012). No pulsars are known to be coincident with NVSS J1957+35. One should look for possible pulsed emission at the location of NVSS J1957+35.

Since the source is located just 3.3° far from the Galactic plane, it is more likely that NVSS J1957+35 is a Galactic source but one can not rule out the completely possible extra-galactic origin of the source.

Variations in the light curve of NVSS J1957+35 could also be due to some kind of extreme scattering of the incident radiation in the interstellar medium of our Galaxy (e.g, Rickett, 1990; Dennett-Thorpe and de Bruyn, 2002; Bannister et al., 2016). Variation from less than few days time-scale (Dennett-Thorpe and de Bruyn, 2002; Rickett, 2002) to year time scale (Gaensler and Hunstead, 2000; Ofek and Frail, 2011) can occur due to interstellar scintillation in GHz frequencies. Since NVSS J1957+35 showed a variation of different time-scales, from minutes to months, and no other nearby radio sources were showing such variabilities, even if interstellar scattering play some role, it is unlikely that all these variations are due to the scattering effect.

If we consider a two component accretion flow where the Keplerian disk is flanked by a transonic flow in hard states when jets are stronger (Chakrabarti and Titarchuk, 1995), it is well known that the Keplerian disk does not have to penetrate distances close to the black hole and the X-ray could be faint. We postulate that the disk with very low accretion rate could be located at a large distance with inner edge $\sim 20,000$ Schwarzschild radii or more so that the source is presently having a quiescence stage, as far as X-rays is concerned. If this is the case, occasional outbursts every few to few tens of years are possible and one could look for them. It is also possible that the disk is shrouded by copious winds from the companion, much like SS 433 (Margon, 1984; Clark, 1984), where disk X-ray is completely blocked. However, in that case, a profusely mass-losing star would be expected in the vicinity. As discussed in Section 3.4, it is possible that 2MASS J19575420+3535152 is the IR counterpart. In fact, the circularly polarized emission is an indication of aligned magnetic fields. If there is an outflow with a small inclination angle with the line of sight, a polarization fraction similar to those reported in Section 3.3 can be produced from its radio emission (viz. Chrysostomou et al., 1997).

4.2. Comparison with Galactic center transients

There are a number of similarities between the temporal evolution of NVSS J1957+35 to that of GCRT J1742-3001 and a transient radio source detected close to Galactic Center region (GCT). While GCRT J1742-3001 was detected as part of transient search program near the Galactic center region in March 2006 to May 2007 at 235 MHz (Hyman et al., 2009), GCT was detected in monitoring observations of Sgr A* from December 1990 to September 1991 at different radio wavelengths from 1.3 to 22 cm (Zhao et al., 1992). There are also some similarity with another transient GCRT J1745-3009 (Hyman et al., 2005; Hyman et al., 2007; Roy et al., 2010) located close to Galactic center at 330 MHz.

The most prominent flare of both GCRT J1742-3001 and GCT took about a month to rise while it decayed in about three months. For NVSS J1957+35, we could not catch total rising and fading profile of many flares due to the inadequate sampling rate and data gap, typical rising and fading time was much shorter compared to GCRT J1742-3001 and GCT. NVSS J1957+35 exhibited a higher frequency of such flares unlike other two sources mentioned above. GCRT J1742-3001 also showed fewer small bursts before the main flare and the GCT showed the presence of a significantly intense secondary burst in the 18–22 cm observations about six months after the primary burst. Though GCRT J1745-3009 was detected only three times, it showed intra-day variability with a time-scale of hundreds of second as NVSS J1957+35.

GCRT J1742-3001 peak flux density was $\sim$100 mJy in 235 MHz and peak flux density of GCT was $\sim$1 Jy in the wavelength range of 18–22 cm ($\sim$1.5 GHz) with $\alpha = -1.2$. The peak flux density of individual flares of NVSS J1957+35 varied between 30 and 200 mJy. Since GCRT J1742-3001 had a very steep spectrum ($\alpha \lesssim -2$), its calculated peak flux density at 1400 MHz ($\lesssim 2.8$ mJy) is much fainter than NVSS J1957+35. The peak flux-densities for three detections of GCRT J1745-3009 were $\sim$1 Jy, $\sim$0.5 Jy and $\sim$0.06 Jy in 330 MHz and with measured $\alpha = -13.5$, the calculated peak flux-density at 1400 MHz, corresponding to 1 Jy flux-density at 330 MHz, is only 3 nano Jy which is much less than NVSS J1957+35.

NVSS J1957+35 showed the presence of variable circular polarization as GCRT J1745-3009 (Roy et al., 2010). But for NVSS J1957+35, the maximum detected polarization fraction is only 25% compared to $\sim$ 100% for the case of GCRT J1745-3009. Circular polarization was not reported for the case of GCRT J1742–3001 and GCT.

No X-ray counter-parts were confirmed for the case of GCT, GCRT J1742-3001 and GCRT J1745-3009. NVSS J1957+35 also has no known X-ray counter part. There is some suggestion that GCT may be associated with X-ray binary (Zhao et al., 1992), which is yet to be established.

GCT, J1742-3001 and GCRT J1745-3009 were found close to the Galactic center region but NVSS J1957+35 was found around 71.7 degrees far from the Galactic center and thus its environment is relatively less crowded with less dense interstellar medium but still the source is in the Galactic plane with low Galactic latitude $b = 3.34^{\circ}$. In spite of some similarities, the nature of NVSS J1957+35 is not entirely like any other sources mentioned above, for example, the source is detected many times while other three sources were detected only a few times. Time-scale of flaring activity of NVSS J1957+35 is also not similar to any other sources mentioned above. These hints that the source may be a possible candidate for a new class of transient sources.

5. Conclusions

We found transient nature of a radio source NVSS J1957+35, approximately 24 arcminute far from Galactic micro-quasar Cygnus X-1. The source showed high variability with different time-scales. It varied between less than 1.9 (3σ) mJy to 201 mJy. NVSS J1957+35 also showed high intra-day variability. In one occasion, the source rose from $\sim$15 mJy to $\sim$170 mJy within 700 s. No evidence of periodicity was found in the light-curve of the source. For a limited number of cases, NVSS J1957+35 showed evidence of variable circular polarized emission with V/I vary between 0.14 and 0.17. The source has no known X-ray counter part of the system. 2MASS J19575420+3535152 may be a NIR counterpart of the source. The nature of the source is still unknown. It is unlikely that the system is a normal black-hole X-ray binary but a partially blocked accretion disk by the wind of the companion star could produce such a system. On the other hand, it is also possible that the emission is coming from a foreground flare star. Though NVSS J1957+35 also has some similarities with several Galactic Centre transient sources, it may perhaps be a

member of a new class of transient source. More multi-frequency monitoring is required to know the nature of the source.

Acknowledgement

DP and SP acknowledge the support of MOES fund to carry out this project. We have used data from VLA which is run by The National Radio Astronomy Observatory (NRAO). NRAO is a facility of the National Science Foundation operated under cooperative agreement by Associated Universities, Inc

Appendix A. Flux densities of NVSS J1957+35

In Tables A.3, we have shown flux densities of NVSS J1957+35 during each epoch of observations covering the entire data set we present in this paper. Date in UT and

Table A.3
Flux-densities of J195754+353513.

Date (UT)	Date (MJD)	Flux density (mJy)	VLA configuration	Date	Date (MJD)	Flux density (mJy)	VLA configuration
12/10/83	45619	<3.4	A	25/11/96	50412	<3.0	A
27/10/83	45634	<4.2	A	07/12/96	50424	<5.9	A
13/01/84	45712	34.3 ± 4.2	B	06/01/97	50454	<10.7	A
13/02/84	45743	15.0 ± 1.9	B	19/01/97	50467	<5.7	AB
27/03/84	45786	<6.3	BC	01/02/97	50480	111.1 ± 11.5	AB
01/05/84	45821	22.5 ± 3.9	C	08/02/97	50487	47.6 ± 6.4	AB
06/05/84	45826	53.0 ± 5.6	C	13/02/97	50492	29.9 ± 3.9	B
20/05/84	45826	63.6 ± 6.4	C	20/02/97	50499	48.4 ± 5.5	B
29/05/84	45849	28.2 ± 4.1	C	27/02/97	50506	27.9 ± 3.3	B
02/06/84	45853	91.4 ± 9.6	C	09/03/97	50516	35.5 ± 4.1	B
17/06/84	45868	<8.0	C	16/03/97	50523	52.3 ± 6.4	B
26/06/84	45877	<13.0	CD	22/03/97	50529	42.1 ± 4.5	B
03/07/84	45884	94.6 ± 10.4	CD	31/03/97	50538	22.7 ± 2.5	B
17/07/84	45898	140.0 ± 16.2	CD	05/04/97	50543	14.3 ± 2.1	B
16/08/84	45928	55.4 ± 10.3	D	07/04/97	50545	49.9 ± 5.5	B
10/11/84	46014	<5.2	A	12/04/97	50550	65.3 ± 7.1	B
14/12/84	46048	29.8 ± 7.8	A	18/04/97	50556	12.6 ± 2.0	B
03/02/85	46099	117.7 ± 13.9	A	26/04/97	50564	19.1 ± 2.9	B
02/03/85	46126	120.7 ± 15.8	A	05/05/97	50573	39.7 ± 7.8	B
05/04/85	46160	<4.3	AB	13/05/97	50581	35.1 ± 3.9	B
16/04/85	46171	59.3 ± 6.4	B	29/05/97	50597	<26.5	CB
28/04/85	46183	25.4	B	03/06/97	50602	94.4 ± 10.0	CB
15/05/85	46200	57.3 ± 7.7	B	10/06/97	50609	125.7 ± 13.3	CB
27/05/85	46212	54.2 ± 6.1	B	18/06/97	50617	41.0 ± 4.6	CB
04/06/85	46220	50.0 ± 5.8	B	24/06/97	50623	100.0 ± 10.7	CB
19/06/85	46235	73.9 ± 7.6	BC	03/07/97	50632	47.6 ± 6.2	C
25/10/85	46353	80.6 ± 9.3	CD	05/07/97	50634	82.8 ± 9.3	C
02/12/85	46411	<13.1	D	10/07/97	50639	<17.3	C
16/01/86	46446	<10.5	D	17/07/97	50646	<26.5	C
17/03/86	46506	<5.0	A	24/07/97	50653	58.8 ± 8.4	C
02/04/86	46522	<2.3	A	31/07/97	50660	105.6 ± 12.1	C
08/06/86	46589	<6.5	A	01/08/97	50661	<17.6	C
23/04/88	47274	65.3 ± 7.1	CD	04/08/97	50664	<16.5	C
26/04/88	47277	76.5 ± 7.3	CD	08/08/97	50668	<17.3	C
28/04/88	47279	64.0 ± 6.6	CD	12/08/97	50672	14.9 ± 1.6	C
03/05/88	47284	62.5 ± 6.4	CD	28/08/97	50688	<20.7	C
04/03/90	47954	50.3 ± 5.3	A	31/08/97	50691	<16.5	C
15/03/91	48330	45.7 ± 4.8	D	04/09/97	50695	77.9 ± 8.9	C
16/03/91	48331	63.5 ± 6.5	D	11/09/97	50702	48.0 ± 6.9	C
17/03/91	48332	75.9 ± 8.0	D	17/09/97	50708	63.1 ± 7.9	C
18/03/91	48333	80.7 ± 8.3	D	26/09/97	50717	15.7 ± 2.3	CD
19/03/91	48334	75.2 ± 8.1	D	03/10/97	50724	<7.0	CD
20/03/91	48335	80.5 ± 9.3	D	09/10/97	50730	<4.4	CD
21/03/91	48336	70.9 ± 7.3	D	17/10/97	50738	62.4 ± 6.8	CD
22/03/91	48337	84.0 ± 8.6	D	22/10/97	50743	91.3 ± 9.6	CD
25/03/91	48340	64.8 ± 6.6	D	27/10/97	50748	99.8 ± 10.7	CD
28/04/91	48374	60.6 ± 11.0	D	08/11/97	50760	38.6 ± 4.4	D
30/04/91	48376	70.4 ± 7.3	D	16/11/97	50768	86.7 ± 9.2	D
02/05/91	48378	72.8 ± 7.5	D	23/11/97	50775	66.4 ± 6.8	D
04/05/91	48380	61.2 ± 6.3	D	30/11/97	50782	88.3 ± 9.3	D
05/05/91	48381	51.8 ± 5.3	D	07/12/97	50789	<2.8	D
03/09/96	50329	<4.5	D	15/12/97	50797	65.4 ± 6.7	D

Table A.3 (*continued*)

Date (UT)	Date (MJD)	Flux density (mJy)	VLA configuration	Date	Date (MJD)	Flux density (mJy)	VLA configuration
12/09/96	50338	<13.2	D	24/12/97	50806	<2.8	D
20/09/96	50346	<5.1	D	09/01/98	50822	71.1 ± 7.4	D
06/10/96	50362	<12.0	AD	16/01/98	50829	<3.6	D
18/10/96	50374	<3.8	A	26/01/98	50839	38.7 ± 4.1	D
27/10/96	50383	<3.8	A	01/02/98	50845	51.1 ± 5.3	D
15/11/96	50402	<5.0	A	21/02/98	50865	39.2 ± 12.8	A
01/03/98	50873	<6.0	A	13/10/99	51464	<2.5	AB
07/03/98	50879	<5.4	A	19/10/99	51470	8.9 ± 1.9	AB
13/03/98	50885	<4.7	A	07/11/99	51489	45.9 ± 5.0	B
18/03/98	50890	<3.9	A	27/11/99	51509	43.7 ± 7.3	B
29/03/98	50901	<5.5	A	01/12/99	51513	60.9 ± 6.4	B
09/04/98	50912	<3.1	A	27/12/99	51539	62.7 ± 6.8	B
22/04/98	50925	<3.7	A	09/01/00	51552	21.2 ± 5.5	B
26/04/98	50929	<4.3	A	18/01/00	51561	27.8 ± 5.2	B
03/05/98	50936	<4.3	A	31/01/00	51574	14.7 ± 4.1	B
10/05/98	50943	<2.7	A	03/02/00	51577	55.7 ± 5.9	B
17/05/98	50950	<3.7	A	11/02/00	51585	26.8 ± 3.1	B
22/05/98	50955	<4.4	A	19/02/00	51593	43.6 ± 4.5	BC
31/05/98	50964	<5.4	A	28/02/00	51602	56.7 ± 6.3	BC
07/06/98	50971	<2.3	AB	13/03/00	51616	<2.0	BC
25/06/98	50989	12.8 ± 2.5	AB	17/03/00	51620	39.1 ± 4.1	C
17/07/98	51011	90.1 ± 11.6	B	21/03/00	51624	75.1 ± 9.2	C
23/07/98	51017	186.7 ± 33.7	B	27/03/00	51630	77.2 ± 8.1	C
31/07/98	51025	61.2 ± 7.4	B	27/04/00	51661	71.5 ± 7.5	C
09/08/98	51034	27.1 ± 5.2	B	31/05/00	51695	61.3 ± 6.7	C
23/08/98	51048	45.0 ± 5.2	B	09/06/00	51704	54.5 ± 6.5	C
30/08/98	51055	67.1 ± 7.7	B	16/06/00	51711	159.9 ± 17.2	C
05/09/98	51061	55.9 ± 6.7	B	23/06/00	51718	129.0 ± 14.4	CD
15/09/98	51071	35.5 ± 4.6	B	07/07/00	51732	89.8 ± 9.7	CD
21/09/98	51077	70.9 ± 8.2	B	17/07/00	51742	115.8 ± 12.2	CD
27/09/98	51083	83.4 ± 11.4	B	20/10/00	51837	104.0 ± 14.2	A
22/10/98	51108	87.8 ± 8.9	BC	02/11/00	51850	109.4 ± 15.3	A
30/10/98	51116	61.0 ± 6.7	BC	04/11/00	51852	<3.4	A
13/11/98	51130	73.8 ± 7.9	BC	09/11/00	51857	<7.8	A
30/11/98	51147	98.1 ± 10.6	C	30/11/00	51878	<8.8	A
06/12/98	51153	<27.7	C	03/12/00	51881	<7.7	A
13/12/98	51160	<45.0	C	14/12/00	51892	<7.4	A
13/01/99	51191	78.8 ± 8.5	C	22/12/00	51900	<5.4	A
19/01/99	51197	40.7 ± 5.6	C	12/01/01	51921	<6.2	A
25/01/99	51203	78.0 ± 8.7	C	19/01/01	51928	<4.5	A
31/01/99	51209	75.3 ± 8.4	C	01/02/01	51941	67.0 ± 7.5	AB
28/02/99	51237	<56.2	CD	06/02/01	51946	<9.2	AB
07/03/99	51244	86.5 ± 9.6	D	14/02/01	51954	<10.2	AB
14/03/99	51251	76.7 ± 8.0	D	22/03/01	51990	28.4 ± 3.3	B
24/03/99	51261	175.3 ± 18.2	D	30/03/01	51998	<11.2	B
31/03/99	51268	29.7 ± 6.4	D	06/04/01	52005	<20.0	B
08/04/99	51276	<1.9	D	08/04/01	52007	34.9 ± 5.8	B
24/04/99	51292	50.4 ± 5.3	D	14/07/01	52104	35.1 ± 4.0	C
01/05/99	51299	58.8 ± 8.6	D	04/08/01	52125	65.8 ± 6.7	C
04/05/99	51302	28.4 ± 3.5	D	21/09/01	52173	123.5 ± 12.9	CD
21/05/99	51319	27.5 ± 3.0	D	01/10/01	52183	16.4 ± 1.8	CD
28/05/99	51326	70.4 ± 7.3	D	25/10/01	52207	<9.8	D
04/07/99	51363	<4.4	A	05/11/01	52218	20.7 ± 2.4	D
13/07/99	51372	<4.9	A	12/11/01	52225	41.1 ± 4.8	D
21/07/99	51380	<3.9	A	21/11/01	52234	87.3 ± 8.9	D
26/07/99	51385	<4.1	A	26/12/01	52269	57.1 ± 5.9	D
03/08/99	51393	<4.0	A	25/01/02	52299	200.9 ± 23.5	A
13/08/99	51403	69.7 ± 10.9	A	21/10/02	52568	49.8 ± 5.0	C
22/08/99	51412	<2.6	A	24/10/02	52571	65.8 ± 6.7	C
01/09/99	51422	<4.6	A	27/10/02	52574	35.2 ± 3.7	C
04/09/99	51425	<4.2	A	05/11/02	52583	31.6 ± 3.3	C
30/09/99	51451	<3.2	AB	16/05/03	52775	<11.5	A
05/10/99	51456	<3.9	AB	04/06/03	52794	145.3 ± 16.9	A
06/10/99	51457	48.6 ± 5.5	AB				

Note: 3σ upper limit is mentioned when the source is not detected.

MJD along with corresponding flux-densities is presented in the table. When the source was not detected, we have mentioned 3σ value as upper-limit of the flux density of the source.

References

Bannister, K.W., Murphy, T., Gaensler, B.M., Hunstead, R.W., Chatterjee, S., 2011. A 22-yr southern sky survey for transient and variable radio sources using the Molonglo Observatory Synthesis Telescope. MNRAS 412, 634–664.

Bannister, K.W., Stevens, J., Tuntsov, A.V., Walker, M.A., Johnston, S., Reynolds, C., Bignall, H., 2016. Real-time detection of an extreme scattering event: constraints on Galactic plasma lenses. Science 351, 354–356.

Bassa, C.G., Tendulkar, S.P., Adams, E.A.K., et al., 2017. FRB 121102 is coincident with a star-forming region in its host galaxy. ApJ 843, L8–L13.

Becker, R.H., White, R.L., Helfand, D.J., 1995. The FIRST survey: faint images of the radio sky at twenty centimeters. ApJ 450, 559–577.

Bell, M.E., Murphy, T., Kaplan, D.L., et al., 2014. A survey for transients and variables with the Murchison Widefield Array 32-tile prototype at 154 MHz. MNRAS 438, 352–367.

Bolton, C.T., 1972. Identification of Cygnus X-1 with HDE 226868. Nature 235, 271–273.

Bower, G.C., Plambeck, R.L., Bolatto, A., McCrady, N., Graham, J.R., De Pater, I., Liu, M.C., Baganoff, F.K., 2003. A giant outburst at millimeter wavelengths in the orion nebula. ApJ 598, 1140–1150.

Bower, G.C., Saul, D., Bloom, J.S., Bolatto, A., Filippenko, A.V., Foley, R.J., Perley, D., 2007. Submillijansky transients in archival radio observations. ApJ 666, 346–360.

Bowyer, S., Byram, E.T., Chubb, T.A., Friedman, H., 1965. Cosmic X-ray sources. Science 147, 394–398.

Bridle, A.H., Schwab, F.R., 1999. Synthesis imaging in radio astronomy II. ASP Conf. Ser. 180, 371–381.

Buehler, R., Scargle, J.D., Blandford, R.D., et al., 2012. Gamma-ray activity in the crab nebula: the exceptional flare of 2011 April. ApJ 749, 26–33.

Cabanela, J.E., Humphreys, R.M., Aldering, G., Larsen, J.A., Odewahn, S.C., Thurmes, P.M., Cornuelle, C.S., 2003. The automated plate scanner catalog of the palomar observatory sky survey. II. The archived database. PASP 115, 837–843.

Chakrabarti, S., Titarchuk, L.G., 1995. Spectral properties of accretion disks around galactic and extragalactic black holes. ApJ 455, 623–639.

Chatterjee, S., Law, C.J., Wharton, R.S., et al., 2017. A direct localization of a fast radio burst and its host. Nature 541, 58–61.

Chrysostomou, A., Ménard, F., Gledhill, T.M., Clark, S., Hough, J.H., McCall, A., Tamura, M., 1997. Polarimetry of young stellar objects-II. Circular polarization ofGSS 30. MNRAS 285, 750–758.

Clark, D.H., 1984. The Quest for SS 433. Viking Adult, New York, ISBN 9780140089967.

Condon, J.J., Cotton, W.D., Greisen, E.W., Yin, Q.F., Perley, R.A., Taylor, G.B., Broderick, J.J., 1998. The NRAO VLA Sky survey. AJ 115, 1693–1716.

Cordes, J.M., Lazio, T.J.W., McLaughlin, M.A., 2004. The dynamic radio sky. New Astron. Rev. 48, 1459–1472.

Cutri, R.M., Skrutskie, M.F., van Dyk, S., et al., 2003. VizieR Online Data Catalog: 2MASS All-Sky Catalog of Point Sources (Cutri+ 2003), 2246

Dennett-Thorpe, J., de Bruyn, A.G., 2002. Interstellar scintillation as the origin of the rapid radio variability of the quasar J1819+3845. Nature 415, 57–60.

Frail, D.A., Kulkarni, S.R., Ofek, E.O., Bower, G.C., Nakar, E., 2012. A revised view of the transient radio sky. ApJ 747, 70–81.

Gaensler, B.M., Hunstead, R.W., 2000. Long-term monitoring of molonglo calibrators. PASA 17, 72–82.

Giacconi, R., Murray, S., Gursky, H., Kellogg, E., Schreier, E., Tananbaum, H., 1972. The Uhuru catalog of X-ray sources. ApJ 178, 281–308.

Gies, D.R., Bolton, C.T., 1986. The optical spectrum of HDE 226868 = Cygnus X-1. II Spectrophotometry and mass estimates. ApJ 304, 371–393.

Gregory, P.C., Taylor, A.R., 1986. Radio patrol of the northern Milky Way – a catalog of sources. II. AJ 92, 371–411.

Hallinan, G., Bourke, S., Lane, C., et al., 2007. Periodic bursts of coherent radio emission from an ultracool dwarf. ApJ 663, L25–L28.

Hurley-Walker, Callingham J.R., Hancock, P.J., et al., 2017. GaLactic and extragalactic all-sky murchison widefield array (GLEAM) survey – I. A low-frequency extragalactic catalogue. MNRAS 464, 1146–1167.

Hyman, S.D., Lazio, T.J.W., Kassim, N.E., Ray, P.S., Markwardt, C.B., Yusef-Zadeh, F., 2005. A powerful bursting radio source towards the Galactic Centre. Nature 434, 50–52.

Hyman, S.D., Roy, S., Pal, S., Lazio, T.J.W., Ray, P.S., Kassim, N.E., Bhatnagar, S., 2007. A faint, steep-spectrum burst from the radio transient GCRT J1745–3009. ApJ 660, L121–L124.

Hyman, S.D., Wijnands, R., Lazio, T.J.W., Pal, S., Starling, R., Kassim, N.E., Ray, P.S., 2009. GCRT J1742-3001: A new radio transient toward the galactic center. ApJ 696, 280–286.

Intema, H.T., Jagannathan, P., Mooley, K.P., Frail, D.A., 2017. The GMRT 150 MHz all-sky radio survey. First alternative data release TGSS ADR1. A&A 598, 78–105.

Karpen, J.T., Crannell, C.J., Hobbs, R.W., et al., 1977. Coordinated X-ray, optical, and radio observations of YZ Canis Minoris. ApJ 216, 479–490.

Kazbegi, A.Z., Machabeli, G.Z., Melikidze, G.I., 1991. On the circular polarization in pulsar emissionOn the circular polarization in pulsar emission. MNRAS 253, 377–387.

Kida, S., Niinuma, K., Suzuki, S., et al., 2008. Two strong radio bursts at high and medium Galactic latitude. New Astron. 13, 519–525.

Levinson, A., Ofek, E.O., Waxman, E., Gal-Yam, A., 2002. Orphan gamma-ray burst radio afterglows: candidates and constraints on beaming. ApJ 576, 923–931.

Lorimer, D.R., Bailes, M., McLaughlin, M.A., Narkevic, D.J., Crawford, F., 2007. A bright millisecond radio burst of extragalactic origin. Science 318, 777–780.

Macquart, J., 2014. Optimization of survey strategies for detecting slow radio transients. PASA 31, 31–46.

Marcote, B., Paragi, Z., Hessels, J.W.T., et al., 2017. The repeating fast radio burst FRB 121102 as seen on milliarcsecond angular scales. ApJ 834, L8–L16.

Margon, B., 1984. Observations of SS 433. ARA&A 22, 507–536.

Massaro, F., Giroletti, M., D'Abrusco, R., Masetti, N., Paggi, A., Cowperthwaite, Philip S., Tosti, G., Funk, S., 1984. Observations of SS 433. ApJS 2014 (213), 3–12.

Matsumura, N., Daishido, T., Kuniyoshi, M., et al., 2007. High and low galactic latitude radio transients in the nasu 1.4 GHz wide-field survey. AJ 133, 1441–1446.

Matsumura, N., Niinuma, K., Kuniyoshi, M., et al., 2009. The closely positioned three radio transients in the nasu 1.4 GHz wide-field survey. AJ 138, 787–795.

Metzger, B.D., Williams, P.K.G., Berger, E., 2015. Extragalactic synchrotron transients in the era of wide-field radio surveys. I. Detection rates and light curve characteristics. ApJ 806, 224–247.

Mooley, K.P., Hallinan, G., Bourke, S., et al., 2016. The Caltech-NRAO Stripe 82 Survey (CNSS). I. The pilot radio transient survey in 50 deg^2. ApJ 818, 105–131.

Mirabel, I.F., Rodriguez, L.F., 1998. Microquasars in our Galaxy. Nature 392, 673–676.

Murdin, P., Webster, B.L., 1971. Optical identification of Cygnus X-1. Nature 233, 110.

Murphy, T., Kaplan, David L., Croft, Steve, et al., 2017. A search for long-time-scale, low-frequency radio transients. MNRAS 466, 1944–1953.

Niinuma, K., Asuma, K., Kuniyoshi, M., et al., 2007. A 3 Jy radio burst at a high galactic latitude. ApJ 657, L37–L40.
Ofek, E.O., Frail, D.A., 2011. The structure function of variable 1.4 GHz radio sources based on NVSS and FIRST observations. ApJ 737, 45O–456.
Osten, R.A., Hawley, S.L., Allred, J.C., Johns-Krull, C.M., Roark, C., 2005. From radio to X-Ray: flares on the dMe flare star EV lacertae. ApJ 621, 398–416.
Perley, R.A., Butler, B.J., 2013. An accurate flux density scale from 1 to 50 GHz. ApJS 204, 19–39.
Polisensky, E., Lane, W.M., Hyman, S.D., et al., 2016. Exploring the transient radio sky with VLITE: early results. ApJ 832, 60–69.
Ravi, V., Shannon, R.M., Bailes, M., et al., 2016. The magnetic field and turbulence of the cosmic web measured using a brilliant fast radio burst. Science 354, 1249–1252.
Rengelink, R.B., Tang, Y., de Bruyn, A.G., Miley, G.K., Bremer, M.N., Roettgering, H.J.A., Bremer, M.A.R., 1997. The Westerbork Northern Sky Survey (WENSS), I.A 570 square degree Mini-Survey around the North Ecliptic Pole. A&AS 124, 259–280.
Richards, M.T., Waltman, E.B., Ghigo, F.D., Richards, D.St.P., 2003. Statistical analysis of 5 year continuous radio flare data from persei, V711 Tauri, Librae, and UX Arietis. ApJS 147, 337–361.
Rickett, B., 2002. The role of interstellar scintillation in intraday variations at centimetre wavelengths. PASA 19, 100–105.
Rickett, B.J., 1990. Radio propagation through the turbulent interstellar plasma. ARA&A 28, 561–605.
Rowlinson, A., Bell, M.E., Murphy, T., 2016. Limits on Fast Radio Bursts and other transient sources at 182 MHz using the Murchison Widefield Array. MNRAS 458, 3506–3522.
Roy, S., Hyman, S.D., Pal, S., Lazio, T.J.W., Ray, P.S., Kassim, N.E., 2010. Circularly polarized emission from the transient bursting radio source GCRT J1745-3009. ApJ 712, L5–L9.
Skrutskie, M.F., Cutri, R.M., Stiening, R., et al., 2006. The two micron all sky survey (2MASS). AJ 131, 1163–1183.
Spangler, S.R., Shawhan, S.D., Rankin, J.M., 1974. Short-duration radio flares of UV ceti stars. ApJ 190, L129–L131.
Spitler, L.G., Cordes, J.M., Hessels, J.W.T., et al., 2014. Fast radio burst discovered in the Arecibo pulsar ALFA survey. ApJ 790, 101–108.
Spitler, L.G., Scholz, P., Hessels, J.W.T., et al., 2016. A repeating fast radio burst. Nature 531, 202–205.
Stewart, A.J., Fender, R.P., Broderick, J.W., et al., 2016. LOFAR MSSS: detection of a low-frequency radio transient in 400 h of monitoring of the North Celestial Pole. MNRAS 456, 2321–2342.
Tananbaum, H., Gursky, H., Kellogg, E.M., Levinson, R., Schreier, E., Giacconi, R., 1972. Discovery of a periodic pulsating binary X-ray source in hercules from UHURU. ApJ 174, L143–L149.
Tendulkar, S.P., Bassa, C.G., Cordes, J.M., et al., 2017. The host galaxy and redshift of the repeating fast radio burst FRB 121102. ApJ 834, L7–L14.
Thyagarajan, N., Helfand, D.J., White, R.L., Becker, R.H., 2011. Variable and transient radio sources in the FIRST survey. ApJ 742, 49–63.
Webster, B.L., Murdin, P., 1972. Cygnus X-1-a spectroscopic binary with a heavy companion? Nature 235, 37–38.
Zhao, J.H., Roberts, D.A., Goss, W.M., et al., 1992. A transient radio source near the center of the Milky Way Galaxy. Science 255, 1538–1543.